Early-winter North Atlantic low-level jet latitude biases in climate models: implications for simulated regional atmosphere-ocean linkages

ENVIRONMENTAL RESEARCH
LETTERS

LETTER • OPEN ACCESS

Early-winter North Atlantic low-level jet latitude biases in climate models: implications for simulated regional atmosphere-ocean linkages

To cite this article: Thomas J Bracegirdle *et al* 2022 *Environ. Res. Lett.* **17** 014025

ENVIRONMENTAL RESEARCH
LETTERS

OPEN ACCESS

RECEIVED
17 September 2021

REVISED
7 December 2021

ACCEPTED FOR PUBLICATION
9 December 2021

PUBLISHED
30 December 2021

LETTER

Early-winter North Atlantic low-level jet latitude biases in climate models: implications for simulated regional atmosphere-ocean linkages

Thomas J Bracegirdle[1,*], **Hua Lu**[1] **and Jon Robson**[2]

[1] British Antarctic Survey, Cambridge, United Kingdom
[2] National Centre for Atmospheric Science, Department of Meteorology, University of Reading, Reading, United Kingdom
[*] Author to whom any correspondence should be addressed.

E-mail: tjbra@bas.ac.uk

Keywords: North Atlantic, CMIP6, westerly jet, sub-polar gyre, atmosphere-ocean coupling

Supplementary material for this article is available online

Abstract

Climate model biases in the North Atlantic (NA) low-level tropospheric westerly jet are a major impediment to reliably representing variability of the NA climate system and its wider influence, in particular over western Europe. A major aspect of the biases is the occurrence of a prominent early-winter equatorward jet bias in Coupled Model Inter-comparison Project Phase 5 (CMIP5) models that has implications for NA atmosphere-ocean coupling. Here we assess whether this bias is reduced in the new CMIP6 models and assess implications for model representation of NA atmosphere-ocean linkages, in particular over the sub-polar gyre (SPG) region. Historical simulations from the CMIP5 and CMIP6 model datasets were compared against reanalysis data over the period 1861–2005. The results show that the early-winter equatorward bias remains present in CMIP6 models, although with an approximately one-fifth reduction compared to CMIP5. The equatorward bias is mainly associated with a weaker-than-observed frequency of poleward excursions of the jet to its northern position. A potential explanation is provided through the identification of a strong link between NA jet latitude bias and systematically too-weak model-simulated low-level baroclinicity over eastern North America in early-winter. CMIP models with larger equatorward jet biases exhibit weaker correlations between temporal variability in speed of the jet and sea surface conditions (sea surface temperatures and turbulent heat fluxes) over the SPG. The results imply that the early-winter equatorward bias in jet latitude in CMIP models could partially explain other known biases, such as the weaker-than-observed seasonal-decadal predictability of the NA climate system.

1. Introduction

An accurate representation of the mean state of the atmosphere in climate models is key to capturing the variability related to atmosphere-ocean coupling. Over the North Atlantic (NA), interactions between the mid-latitude low-level westerly jet and sea surface temperatures (SSTs) play an important role in variability and predictability of the region on seasonal to decadal timescales (Yeager and Robson 2017, Sutton *et al* 2018, Simpson *et al* 2019, Ma *et al* 2020). However, the representation of variability of the coupled atmosphere-ocean system in the NA region differs significantly across models, especially on decadal timescales (Zhang and Wang 2013, Wills *et al* 2019, Xu *et al* 2019). Hence, understanding model diversity is important to constrain predictions and projections. A relevant aspect of biases in Coupled Model Inter-comparison Project Phase 5 (CMIP5) climate models is a prominent early-winter equatorward bias in jet latitude, which does not emerge clearly in seasonal means across the canonical winter months of December–February (Hannachi *et al* 2013, Iqbal *et al* 2018). This early-winter bias has received little attention in terms of its implications in model representation of the NA atmosphere-ocean coupling. The extent to which this bias has been reduced in the new CMIP6 model dataset remains to be

examined and additionally whether there have been related improvements in the representation of NA atmosphere-ocean linkages.

Studies based on reanalysis data suggest that from early to late winter the climatological mid-latitude westerly jet exhibits an equatorward shift from ∼49° N in November to ∼46° N in March (Woollings *et al* 2014). Such a shift in jet latitude broadly follows seasonal changes in the mid-latitude storm track over the western NA, which moves equatorward from autumn to late winter in association with seasonal changes in latitude of baroclinicity over the North American continent (Hoskins and Hodges 2019b). This early-to-late winter jet shift is however poorly represented in CMIP3 and CMIP5 models, with systematic equatorward biases in early winter, i.e. November and December (Hannachi *et al* 2013, Iqbal *et al* 2018). A clear mechanism to explain the larger early-winter bias is not identified in these studies.

In terms of CMIP6, recent studies based on middle winter averages indicate that some improvement might be expected relative to earlier model generations. For instance, Simpson *et al* (2020) show that December to February (DJF) winter-mean equatorward jet biases still exist in CMIP6, but with a slight reduction compared to CMIP5. Priestley *et al* (2020) find that the DJF-averaged storm tracks are too zonal and located too far equatorward in both CMIP5 and CMIP6, although the bias is slightly smaller in CMIP6. Davini and D'Andrea (2020) show that winter blocking frequency in the European sector is still under-estimated in CMIP6, although with reduced biases compared to CMIP5 and CMIP3. These studies however did not consider the seasonal progression of the bias and the possible implications in terms of the representation of links between jet variability and heat fluxes (HFs) and SSTs over the NA. In this study, we first assess to what extent CMIP6 models exhibit a reduction in the pronounced early-winter equatorward climatological jet bias that exists in earlier CMIP generations. The results of this assessment show that the bias remains prominent in the CMIP6 ensemble, although slightly reduced compared to CMIP5. A potential cause of these continued biases is identified as too-weak model-simulated lower-tropospheric and surface meridional temperature gradients over the North American continent, consistent with the link suggested by Hoskins and Hodges (2019a).

We then move on to address the question of whether early-winter jet latitude biases (and any potential improvements in CMIP6) have a significant impact on the representation of NA atmosphere-ocean linkages. We address this question by comparing output from the CMIP5 and CMIP6 climate models with the 20th Century Reanalysis Version 3 (20 CRv3). Our focus is on atmosphere-ocean linkages over the sub-polar gyre (SPG) region of the NA. This is a location of strong atmosphere-ocean interaction that is strongly linked to jet variability (Woollings *et al* 2015, Ma *et al* 2020). It is also a crucial region for the formation and variability of North Atlantic buoyancy driven ocean circulation (Xu *et al* 2019, Petit *et al* 2021) and a major source of NA predictability on annual-to-decadal timescales. In terms of jet variability, we focus on speed of the mid-latitude westerly jet rather than latitude, since jet speed variability induces a stronger and more persistent imprint on NA SSTs and correlates strongly with the SPG region on seasonal to multi-decadal timescales (Woollings *et al* 2015, Ma *et al* 2020).

2. Data and methods

2.1. Reanalysis data

The main atmospheric reanalysis dataset used here for evaluating CMIP models is the NOAA-CIRES-DOE Twentieth Century Reanalysis (20CR) Version 3 (20CRv3) (Slivinski *et al* 2019), which is an update on the previous version 2c. Version 3 comprises an increased number of ensemble members (80 from 56) and corrects issues with version 2c such as inaccurate estimates of uncertainty and a bias in sea-level pressure globally in the mid-19th century. Due to remaining uncertainty over corrections of biased ship observations in this period (Slivinski *et al* 2019), only data from 1861 were included here. All 80 ensemble members were used here to provide a measure of reanalysis uncertainty. SST in 20CRv3 is derived from two different datasets, SODAsi version 3 (Giese *et al* 2016) before 1981 and HadISST2.2 (Titchner and Rayner 2014) for 1981 onwards. Monthly mean fields of the following variables were used: zonal wind on 850 hPa, atmospheric pressure at mean sea level, surface (skin) temperature and total turbulent HF (the sum of sensible and latent components). Note that over open ocean, surface temperature is defined as SST. For HF, positive values denote fluxes from the surface upward into the atmosphere. For calculating ocean surface areal mean indices, a land mask was used to mask out land areas. To check robustness of jet diagnostics across different reanalysis datasets, the European Centre for Medium Range Weather Forecasts (ECMWF) ERA-20C reanalysis (Poli *et al* 2016) was also used. ERA-20C spans the period 1900–2010, therefore its use was restricted to robustness assessments. To assess robustness of 20CRv3-derived meridional temperature gradients, the fully comprehensive ECMWF ERA5 dataset (Hersbach *et al* 2020) and its preliminary extension to 1950 (Bell *et al* 2021) were also used since ERA5 directly assimilates observations of temperature. For the meridional temperature gradient diagnostics temperature at 850 hPa (TA850) and 2 m (TAS) were assessed.

2.2. CMIP5 and CMIP6

The climate (2012) model datasets used are the World Climate Research Programme's CMIP5

(Taylor *et al* 2012) and CMIP6 (Eyring *et al* 2016) datasets. The combined CMIP5 and CMIP6 datasets will be referred to hereinafter simply as 'CMIP'. The analysis is based on output form the full complexity 'historical' simulations, which are run using known major climate forcings over the period from the mid 19th century to the present. For a given model, historical simulations are in general run multiple times and these 'realizations' are important for assessing the role of internal climate variability in the historical period. All available models and realizations with the required data are included, as listed in tables 1 (CMIP5) and 2 (CMIP6). The atmospheric fields used are monthly mean zonal wind and temperature on 850 hPa (CMIP variable names 'ua' and 'ta'), atmospheric pressure at mean sea level ('psl') and surface-air (2 m) temperature ('tas'). To mirror the approach used for assessing 20CRv3, monthly mean skin temperature ('ts') was used for SST diagnostics and the sum of sensible and latent components ('hfss' and 'hfls') used for HF. Monthly data spanning years 1861–2005 were extracted, since this is the period of overlapping availability across CMIP historical simulations and 20CRv3. Daily data for the shorter 1950–2005 period were also extracted for more detailed daily jet latitude diagnostics, due to the lack of pre-1950 availability in many CMIP ensemble members, particularly in CMIP5. Land area fraction ('sftlf') was used to mask out land areas in the ocean surface diagnostics.

Table 1. List of CMIP5 models included. The realization numbers are shown for both monthly and daily data. For some models the required daily data were not available, indicated by a '—'.

Model number	Model name	Realization numbers	
		Monthly	Daily
1	ACCESS1-0	1	1
2	ACCESS1-3	1–3	1
3	bcc-csm1-1	1–3	—
4	bcc-csm1-1-m	1–3	1
5	CanESM2	1–5	1
6	CCSM4	1–5	6
7	CESM1-BGC	1	—
8	CESM1-CAM5	1–3	—
9	CESM1-FASTCHEM	1–3	—
10	CESM1-WACCM	1	—
11	CMCC-CESM	1	1
12	CMCC-CM	1	1
13	CMCC-CMS	1	1
14	CNRM-CM5	1–9	1
15	CNRM-CM5-2	1	—
16	CSIRO-Mk3-6-0	1–10	1
17	GFDL-CM3	1–5	1
18	GISS-E2-H-CC	1	—
19	GISS-E2-R	1–2	—
20	GISS-E2-R-CC	1	—
21	HadGEM2-ES	1–4	—
22	inmcm4	1	1
23	IPSL-CM5A-LR	1–6	1
24	IPSL-CM5A-MR	1–3	1
25	IPSL-CM5B-LR	1	1
26	MIROC-ESM	1–3	1
27	MIROC-ESM-CHEM	1	1
28	MIROC5	1–2	1
29	MPI-ESM-LR	1–2	1
30	MPI-ESM-MR	1–2	1
31	MPI-ESM-P	1–2	1
32	MRI-CGCM3	1–2	1
33	MRI-ESM1	1	1
34	NorESM1-M	1–3	1
35	NorESM1-ME	1	—

2.3. Atmospheric circulation indices

The diagnostics used to assess jet speed and latitude are based on the approach used by Bracegirdle *et al* (2018). This draws from the definition of Woollings *et al* (2015), but uses monthly mean data rather than daily data in order to maximise the number of models and realizations available for inclusion. In this method, for each monthly mean field the maximum in the latitudinal profile of zonally-averaged zonal wind at 850 hPa is identified. The zonal averaging is defined over the longitude range 60° W—0° and the value of the maximum defines the jet speed index (JSI) and the latitude of this maximum defines the jet latitude index. Seasonal means are assembled from jet diagnostics calculated from monthly mean fields. A comparison with results based on daily fields in Bracegirdle *et al* (2018) showed that annual to multi-decadal variability in the monthly-derived indices is a close analogue to the daily-derived version. As part of diagnosing CMIP jet latitude biases in more detail, jet latitude diagnostics using daily data following the method of Woollings *et al* (2010) were calculated for the period 1950–2005.

2.4. Ocean surface diagnostics over the SPG

Area-weighted spatial means of sea surface parameters, surface temperature and HF, are defined over the SPG region (45° N–65° N, 60° W–20° W) denoted SST_{SPG} and HF_{SPG}. This box broadly spans the spatial extent of the SPG as identified by Biri and Klein (2019). The southern boundary of the box was chosen to account for annual-decadal variability in SPG location but also balanced against being too far south into other key regions of the NA, in particular the Gulf Stream. Grid boxes with more than 10% land were masked out. Note that since the SST_{SPG} diagnostic is calculated from surface temperature, it will in general include a small number of sea ice surface temperature grid points at the very north of the domain.

2.5. Diagnostics of air-sea linkages

Atmosphere-ocean linkages are assessed here using correlation coefficients between time series of monthly-mean ocean surface diagnostics (SST_{SPG} and HF_{SPG}) and JSI. Time series correlations are presented as r_{ts} = cor(JSI, sfc), where 'sfc' is either

Table 2. As in Table 1, but for CMIP6 models.

Model number	Model name	Realizations	
		Monthly	Daily
36	ACCESS-CM2	1	1
37	ACCESS-ESM1-5	1	1
38	AWI-ESM-1-1-LR	1	1
39	BCC-CSM2-MR	1–3	1
40	CanESM5	1–10 (p1) 1–10 (p2)	1
41	CanESM5-CanOE	1	—
42	CESM2	1–11	1
43	CESM2-FV2	1	1
44	CESM2-WACCM	1–3	1
45	CESM2-WACCM-FV2	1	1
46	CMCC-CM2-HR4	1	—
47	CMCC-CM2-SR5	1	—
48	CMCC-ESM2	1	—
49	CNRM-CM6-1	1–10	1
50	CNRM-CM6-1-HR	1	—
51	CNRM-ESM2-1	1-5	1
52	FGOALS-g3	1	1
53	GFDL-CM4	1	1
54	GFDL-ESM4	1	—
55	GISS-E2-1-G	1–8	1
56	GISS-E2-1-G-CC	1	—
57	GISS-E2-1-H	1–8	—
58	HadGEM3-GC31-LL	1–4	1
59	HadGEM3-GC31-MM	1–4	1
60	INM-CM5-0	1	1
61	IPSL-CM6A-LR	1–9	1
62	MIROC-ES2L	1	—
63	MPI-ESM1-2-HR	1	1
64	MPI-ESM1-2-LR	1	1
65	MPI-ESM-1-2-HAM	1	1
66	NESM3	1	—
67	NorCPM1	1	—
68	NorESM2-LM	1	1
69	NorESM2-MM	1	1
70	SAM0-UNICON	1	1
71	TaiESM1	1	1
72	UKESM1-0-LL	1–14, 16	1

SST_{SPG} or HF_{SPG}. For example, correlations between JSI and SST_{SPG} for January are calculated from year-to-year time series of January-mean values. All time series are linearly de-trended before calculation of correlations. Although time series correlation is indicative of coupling, it is recognised that it does not quantify atmosphere-ocean interactions in a strict sense.

Correlation is also used to quantify linear associations in CMIP cross-model scatter plots between two variables, denoted r_{cm}. For example, cross-model relationships between climatological jet latitude and time series correlation diagnostics (r_{ts}) are examined to help establish whether atmosphere-ocean linkages are weaker or stronger in models with more equatorward climatological mean jet latitudes.

3. Results

3.1. Early winter climatological jet latitude in CMIP5 and CMIP6

In this section we assess whether the systematic early-winter equatorward bias in jet latitude that exists in previous model generations is also present in CMIP6. Figure 1 shows October to March climatological mean jet latitude. It is evident that the early-winter equatorward bias does indeed persist in CMIP6, which is reflected in spatial maps of climatological low-level winds (figure S1 available online at stacks.iop.org/ERL/16/014025/mmedia). A shorter 1900–2005 period is shown in figure 1(b) to allow the inclusion of ERA20C and demonstrates agreement with 20CRv3. The reanalysis-derived climatological jet latitude exhibits an overall equatorward shift from ∼50° N in October to ∼46° N in March. In comparison, both CMIP ensembles exhibit a more rapid equatorward shift of the jet from October to November. As a result almost all CMIP model realizations exhibit equatorward climatological jet latitude biases in early winter, with ensemble mean biases of 3.0° (November) and 3.0° (December) for CMIP5 and 2.5° and 2.2° for CMIP6. There is therefore an overall improvement in CMIP6 compared to CMIP5, with proportional reductions in ensemble mean equatorward jet latitude bias of 18% and 26% in November and December respectively. In late winter the ensemble mean biases are smaller, but with a larger inter-model spread.

To evaluate the early-winter jet latitude bias in more detail, the frequency distribution of daily jet latitude anomalies from ten day low-pass filtered daily data for November-December is shown in figure 2. Figure 2(a) shows the high latitude peak (at ∼58°–60° N) dominating in 20CRv3. At lower latitudes there are indications of the central and southern peaks of the tri-modal structure that is prominent in winter months (DJF) (Woollings *et al* 2010) (figure 2(b)), but this is less distinct in early winter. It is also apparent from figure 2 that in general this high latitude peak is not reproduced in CMIP historical simulations and that they exhibit an overly dominant central peak at ∼45° N. With regard to interactions with the SPG, this is highly relevant since the position of the northern peak (∼58°–60° N) coincides with latitudes of the SPG (45°–65° N). Consistent with the results for the mean jet latitude (figure 1), there is some improvement in CMIP6 compared to CMIP5 in terms of the relative strengths of the central and northern preferred jet locations. Note that a version of figure 1(b) for the shorter 1950–2005 period used in figure 2 is shown in supplemental material (figure S2) and reproduces the pronounced early-winter equatorward bias in jet latitude.

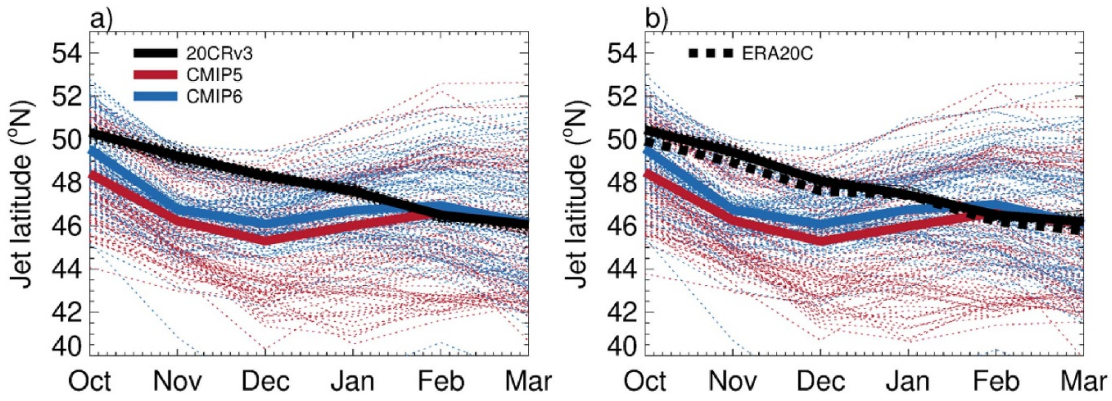

Figure 1. Monthly climatological jet latitude over the period (a) 1861–2005 and (b) 1900–2005. The thick black solid line shows the 20CRv3 ensemble mean with the 80 ensemble members shown by thin black dotted lines (note that these are mainly obscured by the thick black line due to close agreement between members). The thick black dotted line in (b) shows calculations from the ERA20C reanalysis. The thin dotted lines show historical ensemble members from CMIP5 (red) and CMIP6 (blue) with ensemble mean values in thick solid lines.

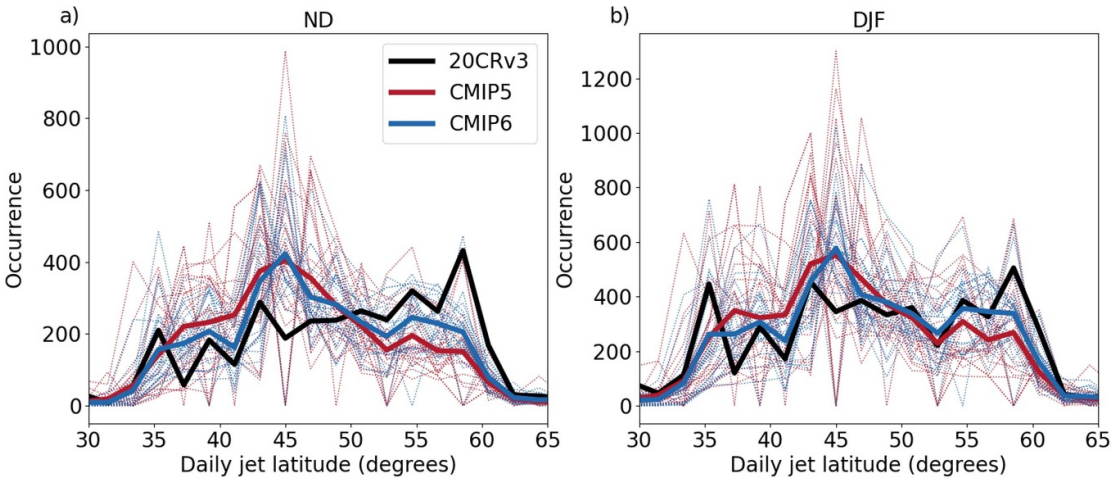

Figure 2. (a) Early winter (ND) and (b) winter (DJF) distributions of jet latitude calculated from daily data smoothed with a ten day Lanczos filter. The thin red and blue dotted lines show individual model ensemble members from historical runs of CMIP5 and CMIP6 models respectively, with thick lines showing ensemble means. The 20CRv3 ensemble means are shown by the thick black lines. Calculations are for the period 1950–2005.

Thus, despite improvements in CMIP6, the majority of CMIP6 models still exhibit an equatorward bias in early winter. The main problem seems to be in representing the high-latitude peak in jet occupancy (figure 2). As a starting point to explaining this early winter bias, we assess whether there are biases in climatological upstream lower-tropospheric meridional temperature gradient simulated by the models (also referred to here as baroclinicity) over the North American continent. This region has been identified as a key region for explaining seasonal climatological NA jet shifts (Hoskins and Hodges 2019a).

Figure 3 shows reanalysis-derived climatological 850 hPa temperature (figures 3(a), (c), (e) and its meridional gradient (figures 3(b), (d), (f)) for early, middle and late months of the extended winter season. A distinct region of strong meridional temperature gradient is evident at mid-latitudes over the eastern North American continent and this extends out over Gulf Stream region of the western NA and north across Newfoundland to the southern border of Labrador.

We examined the baroclinic zone upstream of the NA jet, over eastern North America, and found that early-winter biases in meridional temperature gradient are largest on its poleward side, shown by box A in figure 3 (90°–70° W, 45°–55° N). Two key reasons that one might expect the region on the poleward flank of the baroclinic zone to be important for NA jet latitude are: (a) theoretical/idealised studies have shown that shifts in jet latitude are more strongly associated with shifts in the region of maximum baroclinicity than strengthening/weakening of an existing maximum (Baker *et al* 2017) and (b), consistent with this, (Hoskins and Hodges 2019b) found that summer baroclinicity is centred on this region along with a more poleward position of the NA storm track during summer months (see also figure S3). Here, we

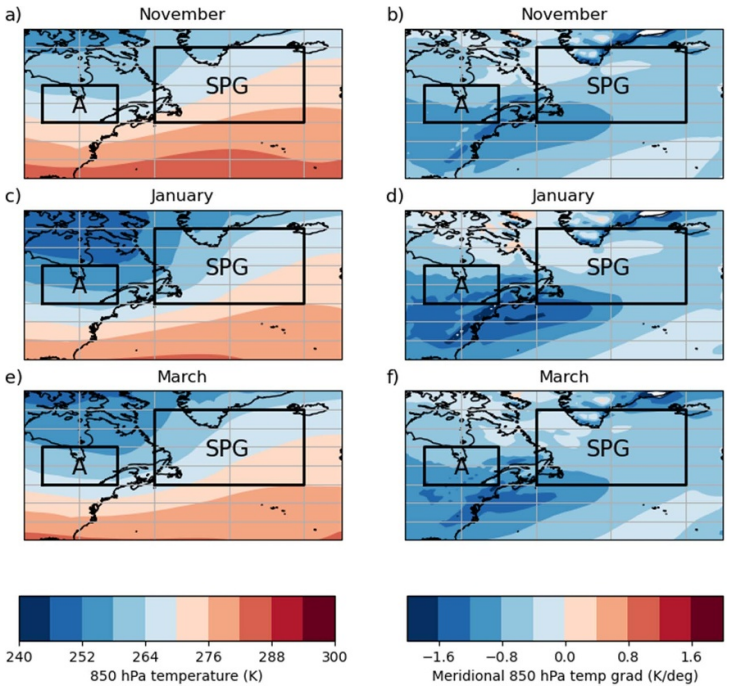

Figure 3. Reanalysis-derived monthly mean climatological 850 hPa temperature (a), (c), (e) and its meridional gradient (b), (d), (f). November, January and March are shown in the top, middle and bottom rows respectively. The reanalysis dataset used is 20CRv3 the multi-year means over the period 1950–2005 are shown. The boxes show regions referred to in the text.

examine whether meridional temperature biases in this region in CMIP models might help to explain the early-winter latitude biases of the NA jet further downstream. For reference the box used define the SPG region is also shown in figure 3.

Figure 4 shows that both CMIP5 and CMIP6 models systematically exhibit too weak 850 hPa meridional temperature gradients in Region A that are most pronounced in early winter (November and December), though the biases are on average slightly smaller in CMIP6. The ensemble mean model biases gradually reduce to small values in March. This early-to-late winter evolution closely reflects the evolution in latitude biases of the NA jet further downstream (figure 1).

The association across the CMIP models between meridional temperature biases in Region A and jet biases is investigated in figure 4(b). This shows only the models with the ten most poleward and ten most equatorward jet latitudes and demonstrates a clear pattern whereby models with stronger climatological baroclinicity (more negative gradients) in region A exhibit more poleward jet positions and vice versa.

Although these upstream biases in low-level baroclinicity are indicative of a causal link, more detailed investigations such as sensitivity experiments would be required make definitive conclusions. However, one key driver of baroclinicity is surface air temperature (TAS) gradients, which are influenced by surface processes and features including snow cover. Figures 4(c) and (d) confirm significant model biases in surface temperature gradients, with a similar winter evolution in meridional gradient bias to that seen at 850 hPa. Reanalysis-derived gradients are more clearly outside the range of the CMIP models in November and December (figure 4(c)). Since 20CRv3 does not assimilate temperature observations, results are also shown in figure 4(c) for the fully-comprehensive ERA5 reanalysis. There is strong agreement between ERA5 and 20CRv3, although ERA5 produces slightly stronger meridional gradients in TAS (figures 4(c) and (d)).

Overall, the more prominent biases in higher-latitude aspects of the NA jet further motivate a focus on the SPG region in terms of the representation of NA ocean-atmosphere interactions.

3.2. Implications of jet latitude bias for atmosphere-ocean linkages

In this section the impacts of the early winter bias in jet latitude on jet-SST linkages over the SPG are assessed. In particular, we focus the question of whether models with mean jet positions further equatorward exhibit weaker jet-SST correlations than those with more poleward jet positions.

To set a baseline for comparison with CMIP data, figure 5 shows reanalysis-derived spatial maps of correlations between year-to-year time series of JSI and ocean surface variables at each grid point for each month of the extended winter from November through March. This shows that the previously-documented significant correlations between JSI and surface parameters over the SPG region (e.g. Woollings *et al* 2015, Ma *et al* 2020) extend to the

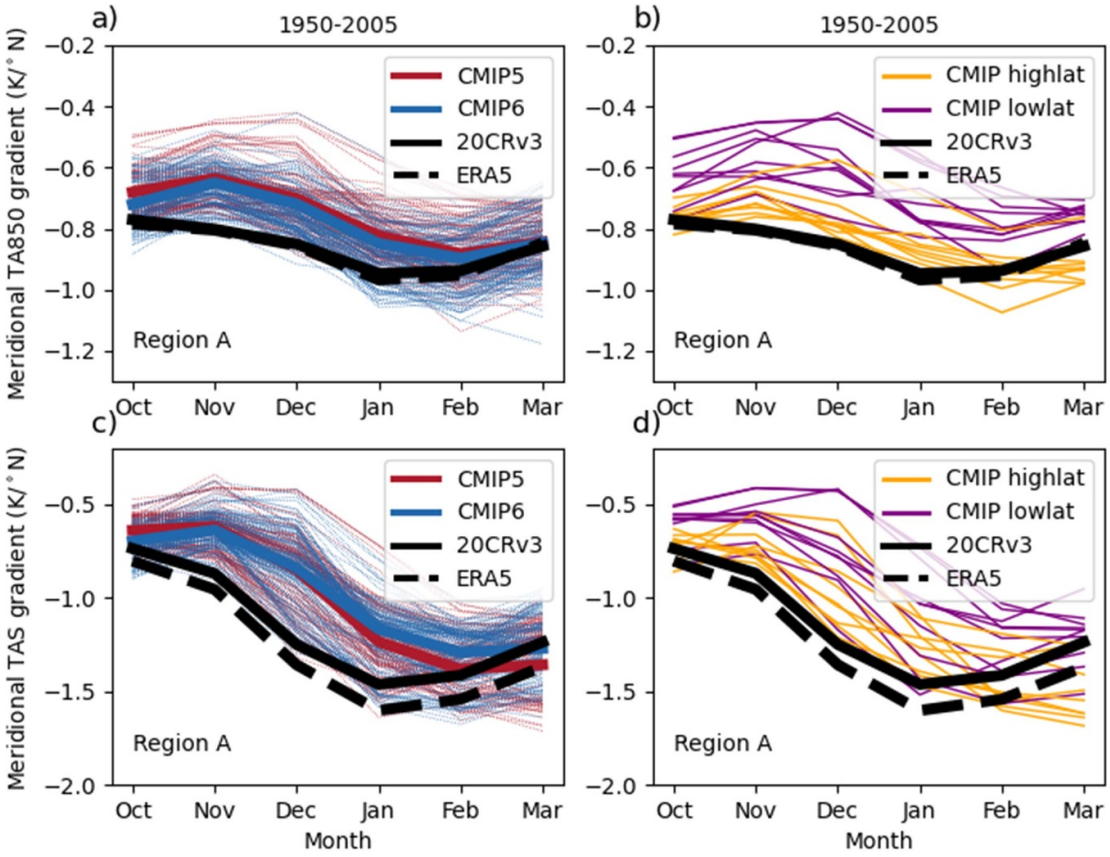

Figure 4. Reanalysis and CMIP meridional temperature gradients over region A (see figure 3). In all panels the thick back solid lines denote 20CRv3 and the dashed black lines show ERA5. In (a) and (c) the thin dotted red and blue lines show CMIP5 and CMIP6 ensemble members respectively (with thick solid lines showing ensemble means). In (b) and (d) the coloured lines show CIMP model realization means (for models with more than one realization) of the models with the 10 most poleward (orange) and equatorward (purple) jet latitudes. All diagnostics are for the period 1950–2005.

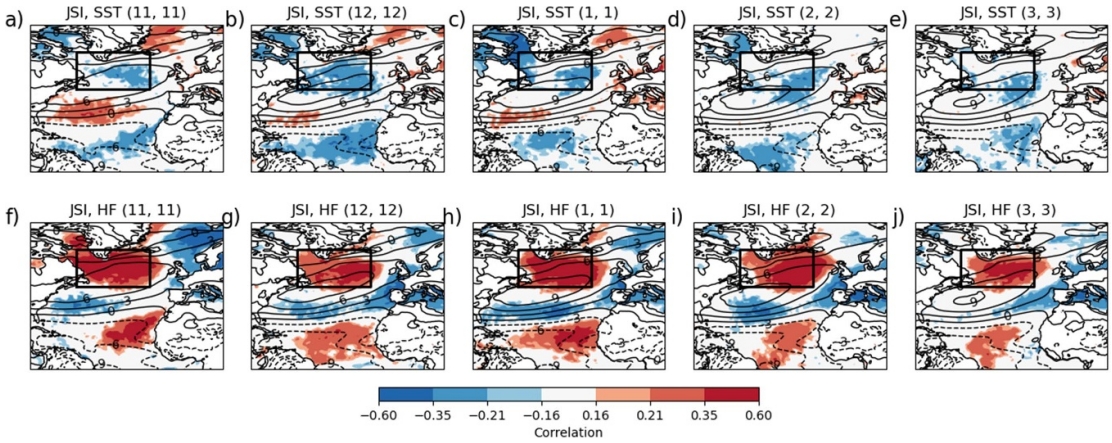

Figure 5. Spatial maps of correlations between time series of JSI and surface variables at each grid point from 20CRv3 over the period 1861–2005 (shading). The upper and lower rows show correlations for skin temperature and HF respectively. Each month in the extended winter season between November to March is shown in each column from left to right. The two smallest correlation contour intervals at ± 0.16 and ± 0.21 are at the $p = 0.05$ and $p = 0.01$ significance levels respectively. The line contours show climatological zonal wind at 850 hPa with contour intervals of 3 m s^{-1} and negative values shown by dashed lines. The black boxes shows the SPG region.

early winter months in which climatological jet latitude biases are most pronounced. Correlations based on SST anomalies from one month later (e.g. time series of January JSI and February SST) show qualitatively similar results (figure S4). This implies that the correlations in year-to-year variability over the SPG region are dominated by the ocean responding to atmospheric variability. The heat loss and cooling over the SPG under strong jet conditions are associated with strong winds and cold air advection

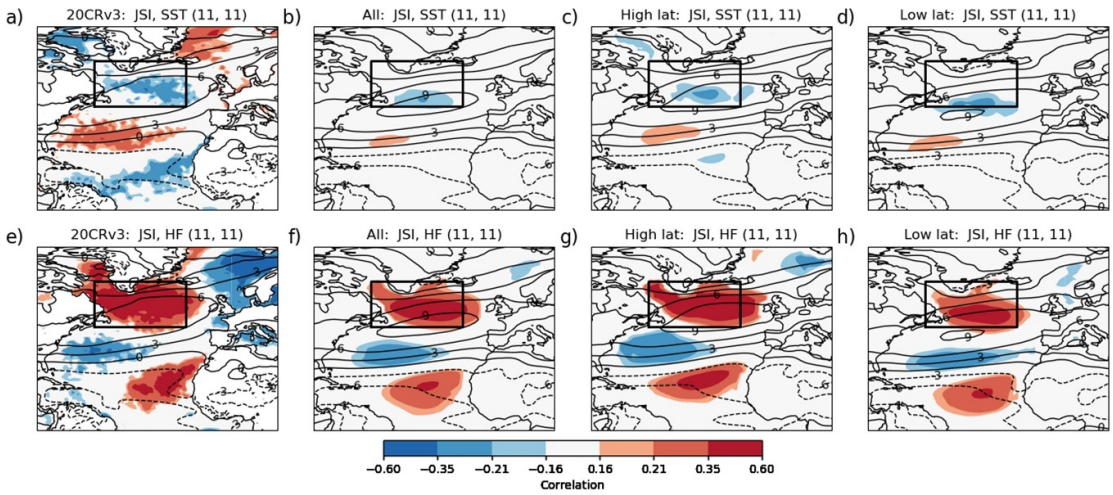

Figure 6. Panels (a) and (e) repeat figures 5(a) and (f) in order to aide comparison with equivalent November plots from CMIP. The other panels show output from CMIP. Specifically CMIP ensemble means (b), (f), sub-ensemble means from models with the ten most poleward climatological jet latitudes (c), (g) and the models with the ten most equatorward climatological jet latitudes (d), (h).

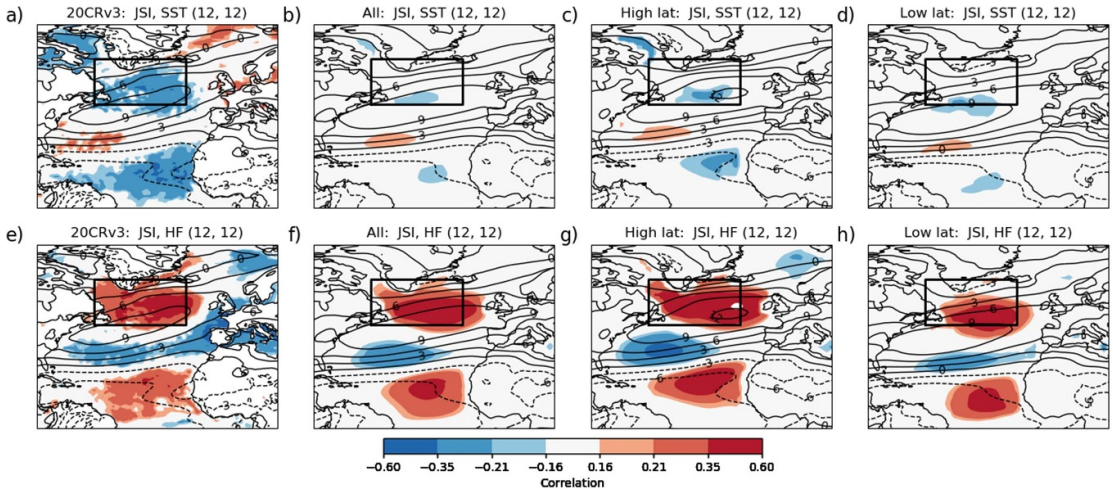

Figure 7. As in figure 6 but for December.

over central-eastern part of the climatological jet (figure 5), with the region of cold-air advection extending to the seas around Greenland (for details see Ma *et al* (2020)).

Equivalent calculations were conducted for each available realization of historical CMIP model simulations, with results for November averaged across all models shown in figure 6 and December in figure 7. Focussing initially on SST over the SPG region, it is evident from figures 6(b) and 7(b) that the main region of negative correlations is located towards the southern boundary of the SPG box in the CMIP ensemble mean. In contrast, the reanalysis correlations are confined to the centre of the box and extend further north into the western Greenland Sea and Labrador Sea.

Selecting subsets of CMIP models with high and low latitude climatological jets demonstrates a link between climatological jet bias and the position of the spatial correlations (figures 6(c), (d) and 7(c), (d)). Models with the ten most equatorward jets (figures 6(d) and 7(d)) show negative correlations shifted further equatorward with the jet and vice versa for those with the ten most poleward jets. Correlations with one-month lagged SST show qualitatively similar results, but more pronounced in association with larger correlation magnitudes over the SPG region (see figures S4–S6). Indeed, the CMIP models with more poleward jets exhibit a closer similarity to reanalysis output, with the main area of negative correlations located centrally within SPG box and regions of negative correlation to the west of Greenland (figures 6(c) and 7(c)). Taking a broader perspective, it is perhaps unsurprising that the NA correlation pattern is in general located further south in the subset of models with more equatorward

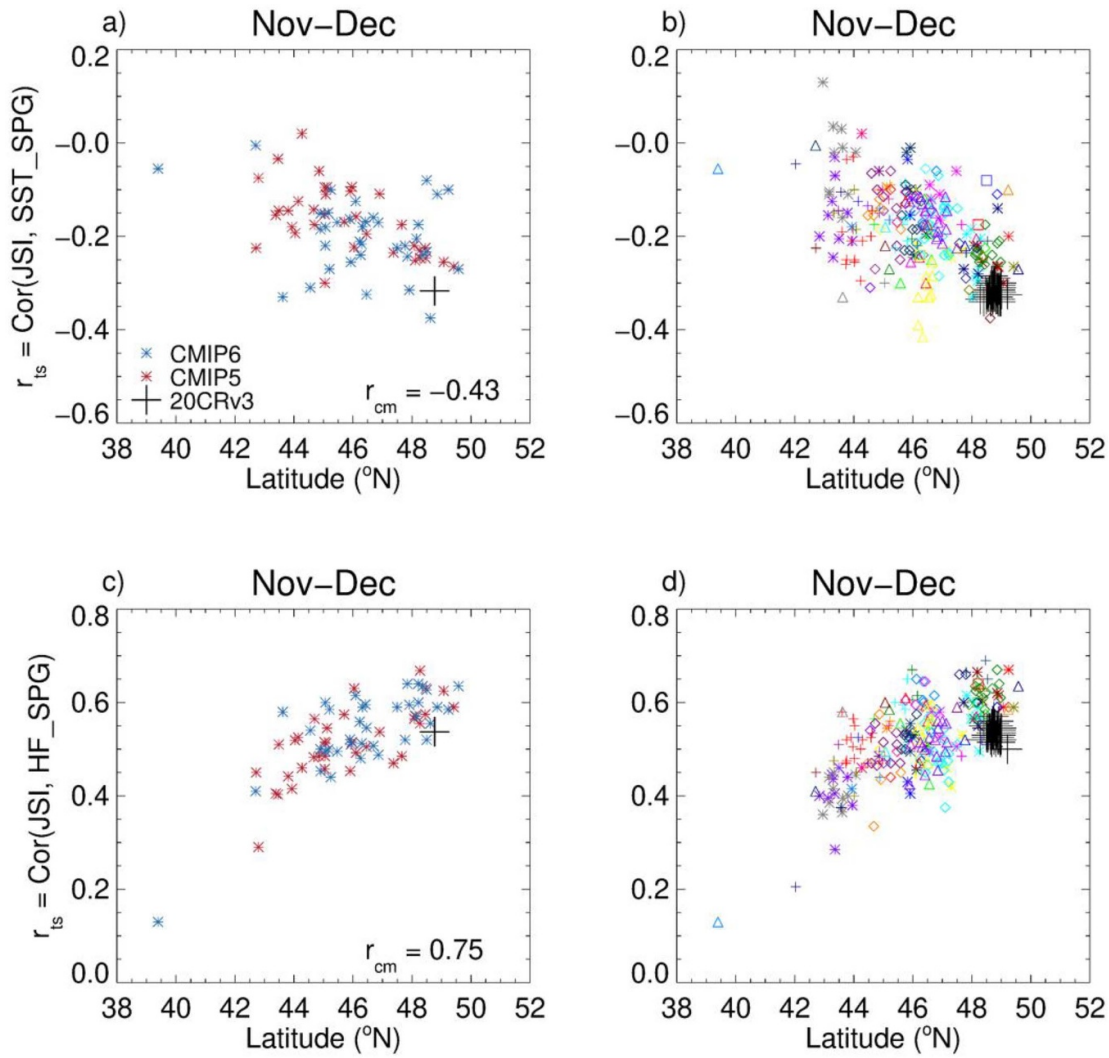

Figure 8. Scatter plots between climatological jet latitude (*x*-axis) and atmosphere-ocean time series correlations (*y*-axis) for early winter (November–December). In (a) and (c) each asterisk represents the realization mean from each CMIP model, with red asterisks showing CMIP5 and blue showing CMIP6, and the black cross shows the 20CRv3 ensemble mean. In (b) and (c) all CMIP and 20CRv3 ensemble members are shown, for which each symbol/colour combination represents an individual CMIP model and the large black crosses show 20CRv3 as for (a) and (c).

climatological jet latitudes. Correlations with one-month lagged SST again show qualitatively similar results, but with larger correlation magnitudes over the SPG region (see figures S4 and S5).

With regard to time series correlations between JSI and turbulent HF, the results are qualitatively similar (lower rows of figures 5–7). In particular, models with more equatorward jets have JSI-HF correlation patterns that are further south in the SPG, and in the models with more poleward (and less biased) jets these patterns look more like the reanalysis. This qualitative consistency, along with the stronger correlations for HF, provides further evidence for the extent of impacts of climatological jet latitude biases on atmosphere-ocean interaction over the SPG and more widely across the NA. Since we find that the CMIP6 models exhibit some improvement over CMIP5 in terms of early-winter jet latitude bias, the results in figures 6 and 7 suggest that this may have translated into a small improvement in representation of JSI-ocean linkages over the SPG.

To explore the relationship between climatological jet latitude and JSI-SPG time series correlations in more detail, scatter plots are shown in figure 8. These demonstrate that, compared to reanalysis data, most CMIP models exhibit weaker JSI-SPG time series correlations associated with the systematic early-winter equatorward jet biases. There is no clear difference in behaviour between the CMIP5 and CMIP6 models, although a larger proportion of CMIP5 models occupy the low-latitude/weak correlation quadrant of the scatter plots.

Potential impacts of sampling uncertainty on the above results are evident in figures 8(b) and (d). Here the within-model spread (i.e. the spread across realizations for a specific model) in output from models with a large number of historical realizations shows that there is a non-negligible sampling uncertainty

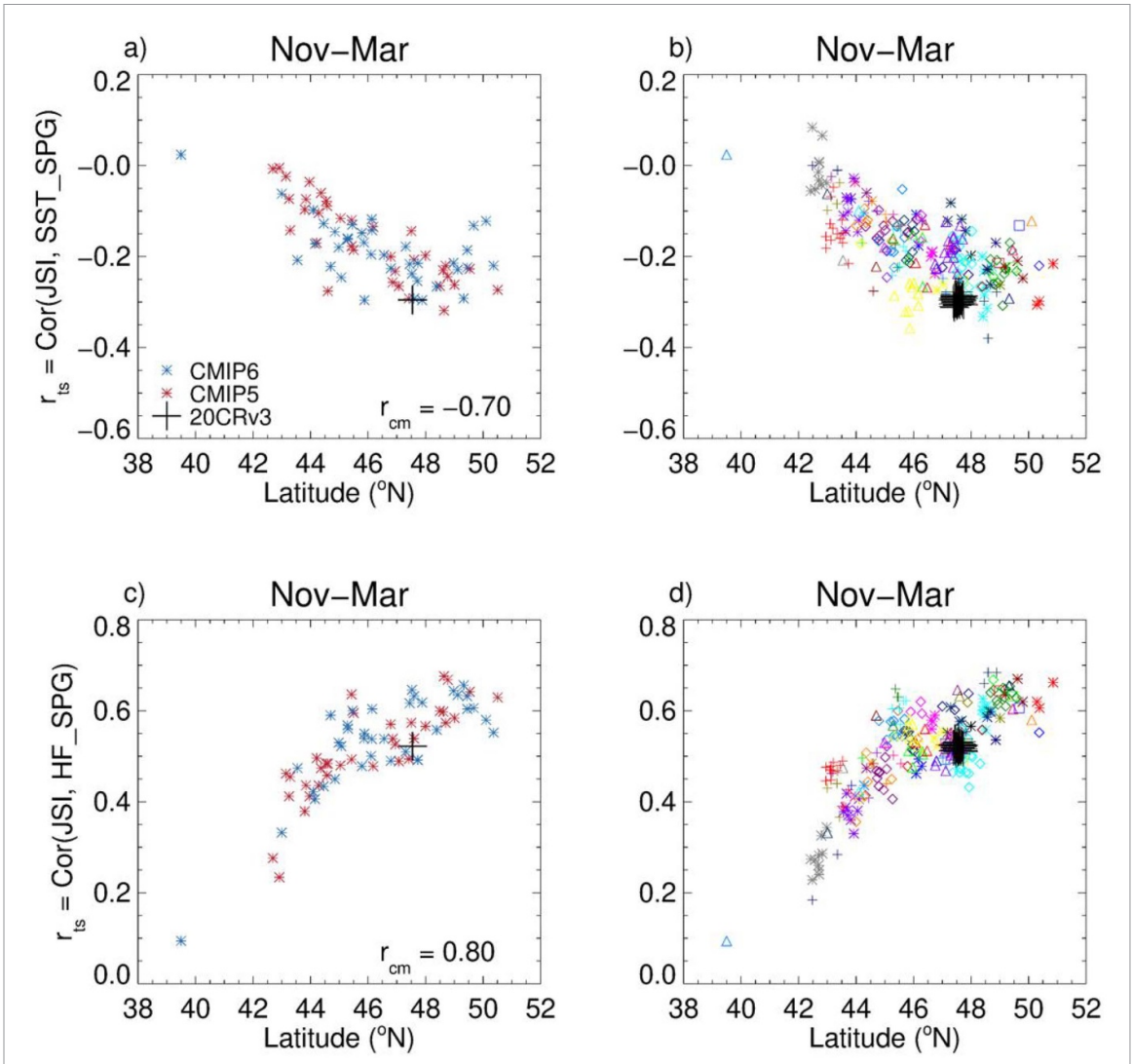

Figure 9. As in figure 8, but for the extended winter (November through March).

for individual realizations. This is mainly related to uncertainty in the time-series correlations (along the *y*-axes), with much smaller within-model spreads for jet latitude (along the *x*-axes). The implication is that associations between jet latitude bias and JSI-SPG time series correlation strength are potentially weaker than they would be if a large number of realizations were available from each model (i.e. reduced sampling uncertainty).

One way to reduce the impacts of sampling uncertainty is to consider the full winter season. Therefore figure 8 was repeated for extended winter (Nov–Mar) diagnostics (figure 9). The broad picture reflects that seen in early winter, with more poleward climatological winter jets generally exhibiting stronger time series correlations between SPG surface variables and JSI. The overall linear cross-model association is clearer than for early winter ($r_{cm} = -0.70$ and 0.80 for SST and HF respectively), which is consistent with the smaller sampling uncertainty of extended winter mean diagnostics (figures 9(b) and (d)). However, the cross-model relationships (r_{cm}) appear non-linear, with stronger sensitivities to latitude in the lower half of the latitude range. This is likely due in part to the regions of stronger JSI-surface correlations extending out of the southern boundary of SPG box in models with more equatorward jet latitudes (e.g. see the early-winter spatial maps in figures 6 and 7). The above scatter plots were repeated with one-month lagged SSTs (e.g. Nov–Dec JSI and Dec–Jan SST), which again show qualitatively similar results but with larger sampling uncertainty and slightly weaker cross-model relationships (figures S7 and S8).

In addition to considering sampling uncertainty, the 80 ensemble members from 20CRv3 are shown individually in figures 8(b) and (d), which provides an measure of the uncertainty in the reanalysis-derived diagnostics. This shows that reanalysis uncertainty is small compared to the spread across different models and between historical realizations of the same model.

4. Conclusions and discussion

In this paper, new reanalysis and climate model datasets (20CRv3 and CMIP6) were used to assess the climate model representation of the North Atlantic tropospheric westerly jet and its linkages to regional ocean surface variability. The main questions addressed are:

- To what extent do CMIP6 models exhibit the pronounced early-winter equatorward climatological jet bias that exists in earlier model generations?
- What are the implications for the representation of NA atmosphere-ocean coupling?

With regard to the first question, we found that the early-winter jet latitude biases still exist in CMIP6, but are reduced compared to CMIP5 by 18% and 26% in November and December respectively. In addition, the early-winter equatorward bias in mean jet latitude is associated with a too-low frequency of excursions to the northern jet location. In winter months (DJF) this northern location is known to be associated with the negative phase of the East Atlantic pattern and increased occurrence of blocking over southwest Europe (Woollings *et al* 2010). However, further research would be required to assess whether this is also the case in early winter. In this regard the recent finding by Davini and D'Andrea (2020), that blocking in the European sector is slightly improved but still under-estimated in CMIP6 models, is consistent with the known link between the NA westerly jet and blocking.

In terms of potential causes of the early-winter jet latitude bias, we show a strong association with upstream meridional temperature gradients over the eastern part of the North American continent. Climatological meridional temperature gradients are systematically too weak in the northern part of the climatological baroclinic zone in early winter, consistent with the stronger equatorward biases in jet latitude. These results highlight the point made by Hoskins and Hodges (2019b), that baroclinicity over terrestrial North America is potentially a key factor in correctly capturing the behaviour of the low-level NA jet, in addition to the influence of SST gradients over the Gulf Stream (e.g. O'Reilly *et al* 2017). The reasons for the model biases in representing low-level and surface temperature gradients in the CMIP models are not clear, but are a priority for future research. More research would also be required to establish the level of causality between upstream meridional temperature gradients over terrestrial North America and jet latitude, or whether other factors are driving the early winter biases in both.

With regard to the second question, CMIP models with lower-latitude jets exhibit lower latitude patterns of correlation between temporal variability in JSI and surface variables over the SPG. In early winter, when equatorward jet biases in CMIP are most pronounced, the results imply an associated weak bias in JSI-SPG linkages in CMIP and a slight reduction in this bias in CMIP6 compared to CMIP5 associated with the slightly reduced ensemble mean jet latitude bias.

The results thus suggest that in early winter the majority of climate models potentially underestimate the strength of impacts on the SPG from jet speed variability. If this is the case, then it would reduce the realism of model-simulated links between SPG variability and atmospheric drivers such as teleconnections to Indian Ocean SSTs (e.g. Bushinsky *et al* 2019) or short-lived climate forcers such as aerosols (Fiedler and Putrasahan 2021). This has relevance for the representation of decadal variability in the NA since, for example, recent modelling evidence shows strong links between Labrador Sea variability and Atlantic thermohaline circulation variability (note that the Labrador Sea is located to the northwest of the SPG region) (Yeager 2020). Indeed, decadal predictability of the SPG in the CMIP6 models has shown improvements compared to CMIP5 due in part to improved variability in SPG SSTs associated with natural forcings such as volcanic eruptions (Borchert *et al* 2021). Whether such improvements in CMIP6 are, at least in part, a result of reduced jet latitude biases is not clear and would require additional analysis.

Further, in terms of the representation of impacts of SPG variability on the atmosphere, it is difficult to provide a clear conclusion from the coupled simulations assessed here. However, other studies have shown weaker jet responses to surface forcing in climate models with climatological mean jets located at lower latitudes. For instance, the seven-model inter-comparison conducted by Ruggieri *et al* (2021) revealed weaker AMV-forced responses in NA midlatitude westerlies in models with lower latitude jets. More broadly, Smith *et al* (2017) found weaker jet responses to anomalous sea ice in models with more equatorward jet latitudes. In the case of sea ice, the early winter biases are of particular relevance since November is the month with largest net energy flux anomalies associated with anomalous sea ice (e.g. Deser *et al* 2010). Both Smith *et al* (2017) and Ruggieri *et al* (2021) invoked internal atmospheric dynamics relating to eddy magnitude and feedback strength to explain weaker responses in models with equatorward latitude biases. Results here additionally highlight that simulated atmospheric responses to SST change in the SPG region are highly sensitive to the relative locations of meridional temperature change and the core of the basic state jet (Woollings *et al* 2012, Gervais *et al* 2019). If models simulate SPG-related surface meridional temperature gradient anomalies too far from the jet core, then atmospheric jet speed responses to anomalous surface temperature could be under-estimated.

In summary, there are a number of challenges in climate modelling for which too weak NA atmosphere-ocean coupling has been suggested as at least part of the explanation. These include weaker-than-observed NA seasonal-decadal predictability, referred to as the signal to noise paradox (Smith *et al* 2020), too-weak low-frequency atmospheric variability in jet speed (Bracegirdle *et al* 2018) and too-weak atmospheric responses to anomalies in surface temperature (Kim *et al* 2018). In this study we have identified a link in CMIP models between systematic equatorward biases in basic state jet latitude and too-weak atmosphere-ocean time series correlations over the SPG. The extent to which this may contribute to the above identified modelling challenges will be an important question in future research, not just for understanding model biases, but also with regard to linking variations in regional atmosphere-ocean coupling with the large decadal variability in mean jet latitude.

Data availability statement

The data that support the findings of this study are openly available at the following URL/DOIs: CMIP5 from https://esgf-node.llnl.gov/search/cmip5/; CMIP6 from https://esgf-index1.ceda.ac.uk/search/cmip6-ceda/; 20CRv3 from https://portal.nersc.gov/project/20C_Reanalysis/; ERA-20C from https://www.ecmwf.int/en/forecasts/dataset/ecmwf-reanalysis-20th-century-using-surface-observations-only; and ERA5 from https://www.ecmwf.int/en/forecasts/dataset/ecmwf-reanalysis-v5.

Acknowledgments

All authors were supported as part of the UK Natural Environment Research Council (NERC) ACSIS project (NE/N018028/1 and NE/N018001/1). TJB and HL were additionally supported through the NERC British Antarctic Survey research programme Polar Science for Planet Earth. JR was additionally supported by NERC via the WISHBONE project (NE/T013516/1) and the National Centre for Atmospheric Science. Three anonymous reviewers are thanked for their excellent suggestions which resulted in many improvements to the manuscript. We acknowledge the World Climate Research Programme, which, through its Working Group on Coupled Modelling, coordinated and promoted CMIP5 and CMIP6. We thank the climate modelling groups for producing and making available their model output, the Earth System Grid Federation (ESGF) for archiving the data and providing access, and the multiple funding agencies who support CMIP5, CMIP6 and ESGF. Support for the Twentieth Century Reanalysis Project version 3 dataset (20CRv3) is provided by the U.S. Department of Energy, Office of Science Biological and Environmental Research (BER), by the National Oceanic and Atmospheric Administration Climate Program Office, and by the NOAA Physical Sciences Laboratory. The Centre for Environmental Data Analysis (CEDA) and JASMIN provided the platform for much of the data analysis conducted.

ORCID iDs

Thomas J Bracegirdle https://orcid.org/0000-0002-8868-4739
Hua Lu https://orcid.org/0000-0001-9485-5082
Jon Robson https://orcid.org/0000-0002-3467-018X

References

Baker H S, Woollings T and Mbengue C 2017 Eddy-driven jet sensitivity to diabatic heating in an idealized GCM *J. Clim.* **30** 6413–31
Bell B *et al* 2021 The ERA5 global reanalysis: Preliminary extension to 1950 *QJR Meteorol Soc* **147** 4186–227
Biri S and Klein B 2019 North Atlantic sub-polar gyre climate index: a new approach *J. Geophys. Res.* **124** 4222–37
Borchert L F, Menary M B, Swingedouw D, Sgubin G, Hermanson L and Mignot J 2021 Improved decadal predictions of North Atlantic subpolar gyre SST in CMIP6 *Geophys. Res. Lett.* **48** e2020GL091307
Bracegirdle T J, Lu H, Eade R and Woollings T 2018 Do CMIP5 models reproduce observed low-frequency North Atlantic jet variability? *Geophys. Res. Lett.* **45** 7204–12
Bushinsky S M, Landschützer P, Rödenbeck C, Gray A R, Baker D, Mazloff M R, Resplandy L, Johnson K S and Sarmiento J L 2019 Reassessing Southern Ocean Air-Sea CO2 flux estimates with the addition of biogeochemical float observations *Glob. Biogeochem. Cycles* **33** 1370–88
Davini P and D'Andrea F 2020 From CMIP3 to CMIP6: Northern Hemisphere atmospheric blocking simulation in present and future climate *J. Clim.* **33** 10021–38
Deser C, Tomas R, Alexander M and Lawrence D 2010 The seasonal atmospheric response to projected Arctic sea ice loss in the late twenty-first century *J. Clim.* **23** 333–51
Eyring V, Bony S, Meehl G A, Senior C A, Stevens B, Stouffer R J and Taylor K E 2016 Overview of the coupled model intercomparison project phase 6 (CMIP6) experimental design and organization *Geosci. Model Dev.* **9** 1937–58
Fiedler S and Putrasahan D 2021 How does the North Atlantic SST pattern respond to anthropogenic aerosols in the 1970s and 2000s? *Geophys. Res. Lett.* **48** e2020GL092142
Gervais M, Shaman J and Kushnir Y 2019 Impacts of the North Atlantic warming hole in future climate projections: mean atmospheric circulation and the North atlantic jet *J. Clim.* **32** 2673–89
Giese B S, Seidel H F, Compo G P and Sardeshmukh P D 2016 An ensemble of ocean reanalyses for 1815–2013 with sparse observational input *J. Geophys. Res.* **121** 6891–910
Hannachi A, Barnes E A and Woollings T 2013 Behaviour of the winter North Atlantic eddy-driven jet stream in the CMIP3 integrations *Clim. Dyn.* **41** 995–1007
Hersbach H *et al* 2020 The ERA5 global reanalysis *Q. J. R. Meteorol. Soc.* **146** 1999–2049
Hoskins B J and Hodges K I 2019a The annual cycle of Northern Hemisphere storm tracks. Part II: regional detail *J. Clim.* **32** 1761–75
Hoskins B J and Hodges K I 2019b The annual cycle of Northern Hemisphere storm tracks. Part I: seasons *J. Clim.* **32** 1743–60
Iqbal W, Leung W N and Hannachi A 2018 Analysis of the variability of the North Atlantic eddy-driven jet stream in CMIP5 *Clim. Dyn.* **51** 235–47

Kim W M, Yeager S, Chang P and Danabasoglu G 2018 Low-frequency North Atlantic climate variability in the community earth system model large ensemble *J. Clim.* **31** 787–813

Ma L P, Woollings T, Williams R G, Smith D and Dunstone N 2020 How does the winter jet stream affect surface temperature, heat flux, and sea ice in the North Atlantic? *J. Clim.* **33** 3711–30

O'Reilly C H, Minobe S, Kuwano-Yoshida A and Woollings T 2017 The Gulf Stream influence on wintertime North Atlantic jet variability *Q.J.R. Meteorol. Soc.* **143** 173–83

Petit T, Lozier M S, Josey S A and Cunningham S A 2021 Role of air-sea fluxes and ocean surface density in the production of deep waters in the eastern subpolar gyre of the North Atlantic *Ocean Sci.* **17** 1353–65

Poli P *et al* 2016 ERA-20C: an atmospheric reanalysis of the twentieth century *J. Clim.* **29** 4083–97

Priestley M D K, Ackerley D, Catto J L, Hodges K I, McDonald R E and Lee R W 2020 An overview of the extratropical storm tracks in CMIP6 historical simulations *J. Clim.* **33** 6315–43

Ruggieri P *et al* 2021 Atlantic multidecadal variability and North Atlantic jet: a multimodel view from the decadal climate prediction project *J. Clim.* **34** 347–60

Simpson I R *et al* 2020 An evaluation of the large-scale atmospheric circulation and its variability in CESM2 and other CMIP models *J. Geophys. Res.* **125** e2020JD032835

Simpson I R, Yeager S G, McKinnon K A and Deser C 2019 Decadal predictability of late winter precipitation in western Europe through an ocean-jet stream connection *Nat. Geosci.* **12** 613–9

Slivinski L C *et al* 2019 Towards a more reliable historical reanalysis: improvements for version 3 of the twentieth century reanalysis system *Q. J. R. Meteorol. Soc.* **145** 2876–908

Smith D M *et al* 2020 North Atlantic climate far more predictable than models imply *Nature* **583** 796–800

Smith D M, Dunstone N J, Scaife A A, Fiedler E K, Copsey D and Hardiman S C 2017 Atmospheric response to arctic and antarctic sea ice: the importance of ocean-atmosphere coupling and the background state *J. Clim.* **30** 4547–65

Sutton R T, McCarthy G D, Robson J, Sinha B, Archibald A and Gray L J 2018 Atlantic multi-decadal variability and the UK ACSIS programme *Bull. Am. Meteorol. Soc.* **99** 415–25

Taylor K E, Stouffer R J and Meehl G A 2012 An Overview of CMIP5 and the Experiment Design *Bulletin of the American Meteorological Society* **93** 485–98

Titchner H A and Rayner N A 2014 The Met Office Hadley Centre sea ice and sea surface temperature data set, version 2: 1. Sea ice concentrations *J. Geophys. Res.* **119** 2864–89

Wills R C J, Armour K C, Battisti D S and Hartmann D L 2019 Ocean-atmosphere dynamical coupling fundamental to the Atlantic multidecadal oscillation *J. Clim.* **32** 251–72

Woollings T, Czuchnicki C and Franzke C 2014 Twentieth century North Atlantic jet variability *Q. J. R. Meteorol. Soc.* **140** 783–91

Woollings T, Franzke C, Hodson D L R, Dong B, Barnes E A, Raible C C and Pinto J G 2015 Contrasting interannual and multidecadal NAO variability *Clim. Dyn.* **45** 539–56

Woollings T, Gregory J M, Pinto J G, Reyers M and Brayshaw D J 2012 Response of the North Atlantic storm track to climate change shaped by ocean-atmosphere coupling *Nat. Geosci.* **5** 313–7

Woollings T, Hannachi A and Hoskins B 2010 Variability of the North Atlantic eddy-driven jet stream *Q. J. R. Meteorol. Soc.* **136** 856–68

Xu X B, Chassignet E P and Wang F C 2019 On the variability of the Atlantic meridional overturning circulation transports in coupled CMIP5 simulations *Clim. Dyn.* **52** 6511–31

Yeager S G and Robson J I 2017 Recent progress in understanding and predicting Atlantic decadal climate variability *Curr. Clim. Change Rep.* **3** 112–27

Yeager S 2020 The abyssal origins of North Atlantic decadal predictability *Clim. Dyn.* **55** 2253–71

Zhang L P and Wang C Z 2013 Multidecadal North Atlantic sea surface temperature and Atlantic meridional overturning circulation variability in CMIP5 historical simulations *J. Geophys. Res.* **118** 5772–91